ORIGINAL ARTICLE

Numerical modeling of free and submerged labyrinth weir flow for a large sidewall angle

José M. Carrillo[1] · Jorge Matos[2] · Ruth Lopes[3]

Abstract

In recent decades, the advancement of knowledge on the hydraulics of labyrinth weirs has resulted mainly from physical modeling. In this study, numerical simulations of free-flow and submerged labyrinth weirs were conducted for a large sidewall angle, using commercially available computational fluid dynamics software, for three different turbulence models. These simulations were compared with experimental data gathered in a fairly large-scale facility. In general, very good agreement was found on the discharge capacity, in free-flow and submerged conditions, regardless of the turbulence model tested. A dimensionless approaching free surface profile, which was virtually independent of the relative upstream head, was obtained. Downstream of the weir, under subcritical flow conditions, the numerical flow depths agreed reasonably well with the corresponding experimental data.

Keywords Labyrinth weir · Discharge coefficient · Submergence · Free surface profile · CFD · Turbulence models

List of symbols

a	Half width of the labyrinth weir apex
C_L	Dimensionless discharge coefficient related to the centerline length of the weir crest L
F_s	Safety factor
g	Gravitational acceleration
H_d	Total downstream head over the weir crestin a submerged condition
H_t	Total upstream head over the weir crestin a free-flow condition

✉ José M. Carrillo
 jose.carrillo@upct.es

 Jorge Matos
 jorge.matos@tecnico.ulisboa.pt

 Ruth Lopes
 r.lopes@hidra.pt

1   Civil Engineering Department, Universidad Politécnica de Cartagena, Cartagena, Spain

2   CERIS, Instituto Superior Técnico, Universidade de Lisboa, Lisbon, Portugal

3   Hidra, Hidráulica e Ambiente, Lda., Lisbon, Portugal

H^*	Total upstream head over the weir crestin a submerged condition
h	Free surface elevation over the weir crest
h_0	Depth of flow over the weir crestin a free-flow condition
L	Total centerline length of the labyrinth weir crest
n	Number of labyrinth weir cycles
P	Labyrinth weir height
p	Pressure
Q	Labyrinth weir discharge
S_M	Momentum source
t	Time
t_w	Vertical thickness of labyrinth weir wall
U	Velocity vector
U_0	Mean velocity upstream of the labyrinth weir
u_i'	Turbulent velocity in each direction (i: 1–3 for x, y, z directions, respectively)
W	Channel width
w	Cycle width of the labyrinth weir
x	Horizontal distance
y_{10}	Characteristic depth where the local air concentration is 10%
y_{90}	Characteristic depth where the local air concentration is 90%
α	Labyrinth weir sidewall angle
δ	Kronecker delta function
ε	Dissipation rate of turbulent kinetic energy
$k = (1/2)\overline{u_i'u_i'}$	Turbulent kinetic energy
μ_t	Eddy dynamic viscosity
ρ	Density
$-\rho\overline{u_i'u_j'}$	Reynolds stress ($i = 1$–3 for x, y, z directions, respectively)
σ	Standard deviation of the relative error of C_L
τ	Stress tensor

1 Introduction

Labyrinth spillways are polygonal overflow weirs folded in plan-view to provide a longer total effective length of the crest for a given overall spillway width. They are usually repeated in modules or cycles. Due to their polygonal shape, labyrinth weirs allow a higher discharge capacity compared with straight overflow weirs for the same width and upstream energy head.

The first labyrinth weir studies seem to have been conducted at the *École des Ponts et Chaussées* (Paris, France) in the middle of the nineteenth century [5]. Those studies considered labyrinths as weirs with a herringbone pattern and compared their behavior with oblique weirs of the same crest length. The advantages of the labyrinth weir, including the weir shape adopted for the reinforced-concrete spillway of the Keno Canal, in the USA, were highlighted by Murphy (1909) [15].

Since labyrinth weirs are relatively low-cost spillways compared to gated spillways, they are often used in conjunction with the raising of dams for increased storage volume [30].

For given values of the design flood and water level in the reservoir, the crest of a labyrinth weir may be placed at a higher elevation than that of a linear weir, thus increasing the storage capacity of the reservoir.

A significant number of experimental studies carried out to date have focused on the influence of geometric factors on the discharge coefficient or the discharge capacity (e.g., [6, 9, 11, 13, 16, 21, 23, 24, 35, 36]). Those studies enabled the determination of the discharge coefficient for certain plan shapes and crest profiles, as a function of the normalized crest development, or of the sidewall angle, and of the hydraulic head over the crest normalized by the weir height.

A limited number of numerical studies have been carried out to date on the hydraulics of non-linear weirs, such as labyrinth weirs (e.g., [4, 28, 29]) or Piano Key weirs (e.g., [7, 12]). The labyrinth weir studies, as well as those of Crookston et al. [7] for Piano Key weirs, were mainly focused on the analysis of the discharge coefficient in free-discharge flow conditions, using different turbulence models. In turn, Denys and Basson [12] used Large Eddy Simulation (LES) models to analyze the flow patterns near the walls of Piano Key weirs, providing an insight on the separation of the flow and the vorticity near the weir.

Notwithstanding the advancement resulting from those studies, the numerical modeling of labyrinth weirs for large sidewall angles and for submerged flow conditions is still lacking. Furthermore, very few studies have focused on the numerical modeling of the complex flow downstream of the weir [32, 33].

In this present work, free and submerged discharge coefficients obtained by Lopes et al. [20] and Lopes [21] in a fairly large size physical model of a labyrinth weir, as well as the submerged hydraulic head relationship, have been analyzed and compared with experimental data and formulae proposed in the literature, for similar quarter-round crests. Subsequently, numerical simulations for 30° sidewall angle using commercially available CFD software are presented and compared with experimental data. The discharge coefficient is analyzed in free and submerged flow conditions. Also, the flow depths upstream and downstream of the weir, under subcritical flow conditions, are computed and compared with experimental data.

2 Previous studies

2.1 Free-flow labyrinth weirs

The discharge capacity of free-flow labyrinth weirs is related to the depth of flow over the weir crest, h_0, or the total upstream head over the weir crest, H_t, the length of the crest, L, and the discharge coefficient, C_L (Fig. 1).

The discharge coefficient is a function of the ratio total head over the weir crest to the weir height ratio, H_t/P, the ratio between the length of the crest and the width of the channel, L/W (magnification ratio), or the sidewall angle, α, the shape of the crest, the characteristics of the inlet channel, and the nappe aeration conditions downstream of the weir (e.g., [9, 13, 24, 35]). Following Crookston and Tullis [9], the head-discharge relationship may be determined using a general form of the linear weir equation:
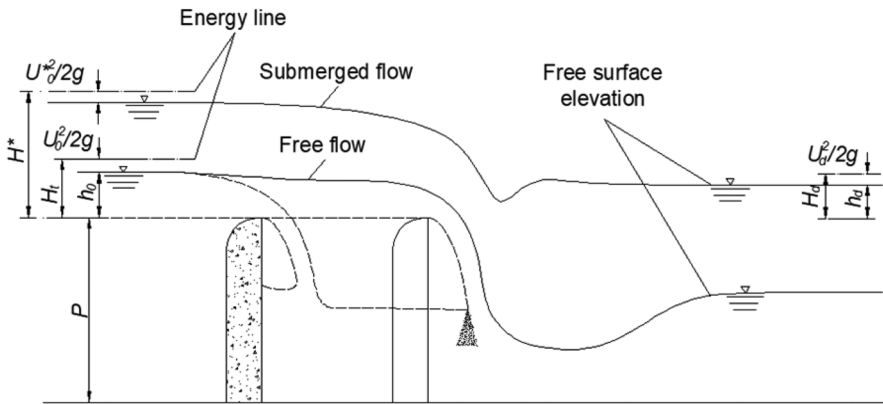
$$Q = \frac{2}{3} C_L L_c \sqrt{2g} H_t^{3/2} \tag{1}$$

Fig. 1 Labyrinth weir scheme for free and submerged flows

where Q = labyrinth weir discharge; C_L = discharge coefficient; L_c = total centerline length of the labyrinth weir crest; g = gravitational acceleration; and H_t = total upstream head over the weir crest, in a free-flow condition.

The influence of the normal (outside apexes connected to channel sidewalls as upstream apexes) or the inverse (outside apexes connected as downstream apexes) orientation of the labyrinth weir on the discharge coefficient has been considered in previous studies. According to Houston [17], labyrinths with a magnification ratio of 5 in the normal orientation were found to discharge up to 9% more than the same weirs in the inverse orientation. However, with the labyrinth projecting into the reservoir in the inverse orientation, discharges were up to 20% greater than in the normal orientation. Crookston and Tullis [9] tested the discharge in normal and inverse orientations with a sidewall angle of 6°. As no measurable variation was observed, the authors considered their results independent of weir orientation. An analogous conclusion was obtained by Lopes [20], by comparing the free-flow discharge coefficient in normal and inverse orientation with sidewall angles of 12° and 30°; the values were fairly similar, with relative differences being lower than 5%.

The influence of the sidewall angle, α, on the discharge coefficient of labyrinth weirs has been studied by several authors. Tullis et al. [35] analyzed labyrinth weirs with a quarter-round crest for sidewall angles between 6° and 18°, and straight weirs (90°). Curves for sidewall angles of 25° and 35° were obtained by interpolation. Two labyrinth heights were considered, 0.152 and 0.229 m, with the weir crest height to wall thickness ratio $P/t_w = 6$. The authors considered the total upstream head and an effective weir length as the characteristic parameters in Eq. (1). A fourth order polynomial fit equation was obtained for each sidewall angle. They also presented a spreadsheet-based tool to design labyrinth weirs with a quarter-round crest.

Willmore [40] tested several shape crests. Quarter-round crest labyrinths were analyzed with sidewall angles of 7° and 8°, and a relative thickness ratio $P/t_w = 8$. The author detected some discrepancies for the smaller sidewall angles and in the formula used to obtain the effective weir length proposed by Tullis et al. [35]. The author also proposed the use of total centerline length instead of the effective crest length of the labyrinth weir crest.

Lopes et al. [21] analyzed the discharge coefficient of inverse oriented, quarter-round crest labyrinths for two sidewall angles, 12° and 30°, on 1 and 2 m wide flumes. The relative thickness ratio P/t_w was 11.9. The labyrinth height was 0.25 m in both cases. No

noticeable differences were observed between the discharge coefficients obtained in both flumes for identical geometric and hydraulic conditions. Values of the discharge coefficient obtained by Lopes et al. [21] were similar to those of Tullis et al. [35], regardless of the total upstream head.

Khode et al. [18] analyzed labyrinth weirs in a 0.30 m wide flume for sidewall angles ranging from 8° to 30°, and straight weirs, both with quarter-round crests. Two labyrinth weir heights were tested, 0.10 and 0.075 m. The P/t_w ratios were 16.7 and 12.5, respectively. A fourth order polynomial fit equation was obtained for each sidewall angle to estimate the discharge coefficient as a function of the effective crest length. Results were compared with seven prototype dam flows, and maximum relative differences were within $\pm 6\%$. Based on the results of Khode et al. [18], new formulae were proposed to explicitly include the sidewall angle [1, 14, 38].

Crookston [6] and Crookston and Tullis [9] considered quarter-round and half-round crest shapes with sidewall angles ranging from 6° to 35°. The labyrinth height was 0.3048 m with $P/t_w = 8$. The authors found that the discharge with a half-round crest was up to 18% greater than that with a quarter-round crest. Considering the effective weir crest length in both cases, good agreement was obtained with the measurements of Tullis et al. [35] for large values of H_t/P. However, large differences were observed for $H_t/P \leq 0.4$. The authors considered that those differences were due to differences in the weir models. The spreadsheet-based labyrinth weir design proposed by Tullis et al. [35] was also updated.

Based on Crookston and Tullis [9] measurements, Vatankhah [37] proposed a general regression expression incorporating the sidewall angle. According to that author, said formula reduces the error using different sidewall angles once the interpolation between different curves is not required.

Figure 2 includes the experimental discharge coefficients obtained by several authors with quarter-round crested weirs considering the total centerline crest length for the
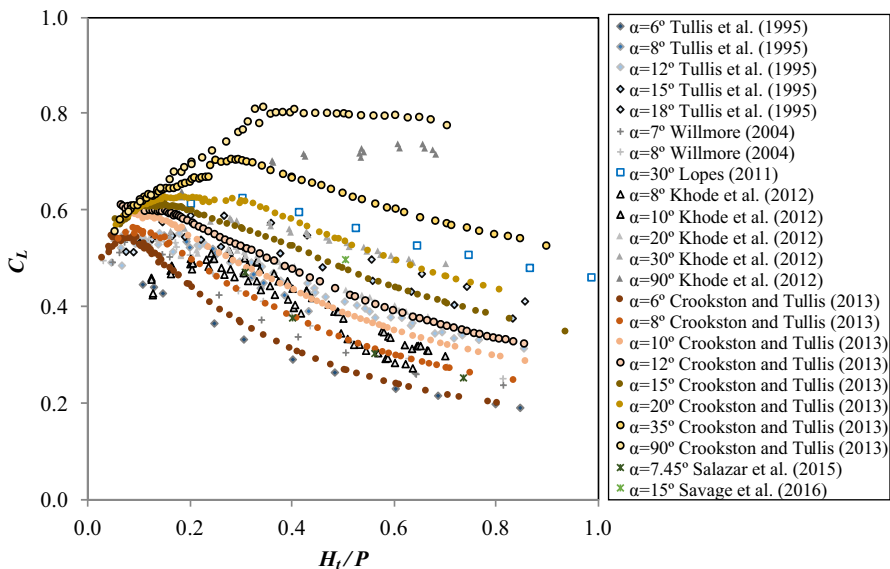

Fig. 2 Values of C_L versus H_t/P, for different sidewall angles with quarter-round crest weirs: experimental test results (Data obtained through digitalization, except for those of Lopes [20])

definition of the discharge coefficient, C_L. The data of Tullis et al. [35], Lopes [20], and Khode et al. [18] were readjusted to consider the total centerline crest length.

The experimental data obtained by Lopes [20] with 30° quarter-round crested labyrinths, in inverse orientation, are generally in agreement with those obtained by other authors, for an identical sidewall angle. The experimental data are between those obtained by Khode et al. [18], for a 30° sidewall angle, and the interpolated results from sidewall angles of 20° and 35° of Crookston and Tullis [9], with average relative differences of 6.8% and 4.4%, respectively, despite the differences in the weir orientation, height and thickness of those studies.

As pointed out by Crookston [6], differences may also be associated with construction quality of the model and turbulence conditions in the approach flow, among others. For low relative heads (e.g., $H_t/P < 0.2$), larger relative differences were found among different experimental studies, possibly also due to scale effects, random errors or dissimilar labyrinth weir geometry (e.g., [13, 34]). Overall, the results of the experimental tests conducted by Lopes [20] were comparable to those gathered on other labyrinth weir studies, for a similar sidewall angle.

Regarding computational fluid dynamics (CFD), few model studies have been carried out thus far (see Fig. 2). Salazar et al. [28] simulated a sidewall angle of 7.45° and obtained reasonably good agreement with the values proposed by Crookston and Tullis [9]. For small H_t/P ratios, the relative differences were around 12%, whereas for H_t/P ratios between 0.4 and 0.8, the differences were around 2%. Savage et al. [29] compared experimental data and CFD simulations to expand the H_t/P range of the 15° sidewall angle fit curve up to 2.1. Relative errors were limited to 6.4% for $H_t/P = 0.502$, and showed a tendency to decrease for larger values of H_t/P. Bilhan et al. [4] analyzed circular labyrinth weirs, by comparing CFD results with their own measurements. The average percentage error between the simulated and observed values was 3.7% for weirs without nappe breakers and 3.0% for weirs with nappe breakers. Recently, Torres et al. [32, 33] conducted 3D CFD simulations of hydraulic flows over a labyrinth weir and spillway using the ANSYS Fluent and OpenFOAM solvers. Overall, good agreement was achieved with the physical model measurements and the consistency in their predictions, namely for water velocity, depth and wave patterns [32]. Also, prototype simulations and comparisons between predictions at the model and prototype scales were conducted for two flow rates. Overall the two solvers predicted the prototype flows to be shallower and with higher velocities than those at model scale, with scale effects becoming less prominent for increasing flow rates. In turn, the wave structures in the prototype presented elongation compared to those at model scale [33].

2.2 Submerged-flow labyrinth weirs

Notwithstanding the considerable number of experimental studies carried out to date on the influence of the submergence in the discharge capacity of straight overflow weirs, few studies have focused on labyrinth weirs. It is likely that this is due to labyrinth structures not usually being designed to work in submergence conditions [24, 31]. However, as the discharge capacity of labyrinth structures is larger than in straight weirs, for the same width and head, there is currently a generalization of their use, and submergence conditions should also be considered [21, 36].

Taylor [31] verified that the water level downstream of the labyrinth structure does not affect the discharge capacity if it is smaller than or equal to the weir height. However, larger downstream water depths lead to a decreasing discharge over the weir.

Tullis et al. [36] carried out a systematic study of submergence. Sidewall angles of 7°, 8° and 20° were considered. Comparing their results for the linear weir flow reduction factor with the Villemonte [39] equation for submerged straight weir flows, the average relative differences were 8.9%, and the maximum relative differences were limited to about 22%. As shown by Tullis et al. [36], the results were in agreement with previous conclusions regarding the accuracy of the Villemonte [39] equation to estimate submerged labyrinth weirs [13, 31].

The influence of submergence was also analyzed by Tullis et al. [36] using the ratio of the total upstream submerged head and total head in free-flow condition, over the weir crest (H^*/H_t) depending on the total downstream head and total upstream head over the weir crest ratio, in free-flow condition (H_d/H_t). The authors proposed three different regression equations with maximum relative differences with the laboratory data of 4.2%. The influence of submergence occurred for $H_d/H_t > 0$, but its effect was relatively small for $H_d/H_t \leq 0.50$ (Fig. 3). For large downstream levels, the labyrinth weir ceased to work as a control structure ($H_d \sim H^*$). Their results suggested that the dimensionless relations were independent of the sidewall angle.

Lopes et al. [21] analyzed the submerged behavior of labyrinth weirs with sidewall angles of 12° and 30° (also plotted in Fig. 3). Measurements were limited to $H_d/H < 1.30$ and $H_t/P \leq 0.80$. The relative differences between H^*/H_t obtained for those sidewall angles, for identical H_d/H_t, were lower than 4%. Further, the relative differences between their results and the formula proposed by Tullis et al. [36] were lower than 6%, for identical H_d/H_t. Based on their results, along with those of Tullis et al. [36], it was suggested that the influence of the labyrinth crest shape, weir orientation and sidewall angle on the dimensionless submerged head should be small, within the range of tested conditions. Hence, the experimental data of Lopes et al. [21], used herein to test the numerical model for submerged flows, are in line to those gathered by Tullis et al. [36], for similar geometric and hydraulic conditions.

Fig. 3 Dimensionless submerged head H^*/H_t versus H_d/H_t for submerged labyrinth weirs (Data obtained through digitalization, except for those of Lopes [20])
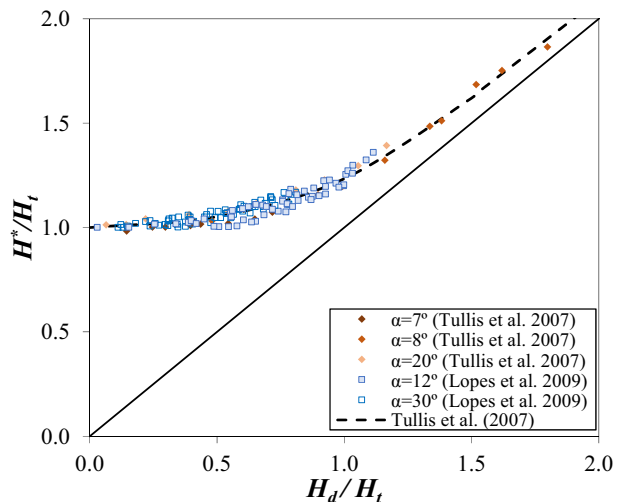
3 Experimental set-up

The experimental data used in this study were acquired on a 41.0 m long, 1.0 m wide and 0.80 m high horizontal flume assembled at the National Laboratory of Civil Engineering (LNEC), Lisbon [20, 21].

Labyrinth weir geometric characteristics and hydraulic conditions were selected to avoid systematic errors, as per Falvey [13]. A trapezoidal labyrinth weir was installed in the inverse orientation with the following characteristics: sidewall angle $\alpha = 30°$; labyrinth weir height $P = 0.25$ m; number of cycles $n = 2$; crest length to flume width ratio, $L/W = 1.80$; width of one cycle to labyrinth weir height ratio, $w/P = 2$. The weir wall thickness was $t_w = 0.021$ m, while the apex was $2a = 0.026$ m. A quarter-round crest profile was considered. The air cavity beneath the nappe was not artificially ventilated.

The water discharge was measured with an electromagnetic flowmeter located in the supply line, with a discharge measurement accuracy of $\pm 0.5\%$. Discharges up to 0.307 m^3/s were investigated, corresponding to Reynolds number on the 1 m wide flume ranging between 0.7×10^5 and 3.8×10^5. The upstream and downstream water levels were measured with point gauges, with ± 0.05 mm resolution. The instrumentation was mounted on a trolley system that enabled longitudinal and transverse translations. The longitudinal and transverse positions were estimated to be accurate to ± 1.0 mm.

Water levels were measured at a section located 0.875 m (3.5P) upstream of the labyrinth weir. Downstream of the weir, water levels were measured at a distance of 2.30 m (9.2P) from the weir. Three different transverse positions were considered, 0.25, 0.50 and 0.75 m from the channel left sidewall, respectively. In free-flow conditions, subcritical flow occurred in the horizontal channel downstream of the labyrinth weir only for $H_t/P > 0.8$.

The characteristic flow depths along the chute, downstream of the labyrinth weir, were also estimated from the air concentration profiles, acquired with a conductivity probe developed by the U.S. Bureau of Reclamation [22, 25]. Taking into account the unsteadiness of the free-surface, maximum, and minimum flow depths were also obtained by visual observation through the sidewalls, using rulers graduated in millimeters.

The experimental setup, instrumentation, and test procedures are discussed in detail in Lopes [20].

4 Numerical model

The Navier–Stokes equations have no known general analytical solution but can be discretized and solved numerically. Three-dimensional CFD codes solve these partial differential equations in each control volume of the fluid domain with different methods.

The ANSYS CFX program (version 18.0) was adopted in order to test its accuracy in solving labyrinth weir hydraulics. The code solves the unsteady Navier–Stokes equations in their conservative form. The instantaneous equations for conservation of mass and momentum may be written as follows, in a stationary frame [2]:

$$\frac{\partial \rho}{\partial t} + \frac{\partial}{\partial x_j}\left(\rho U_j\right) = 0 \tag{2}$$

$$\frac{\partial \rho U_i}{\partial t} + \frac{\partial}{\partial x_j}\left(\rho U_i U_j\right) = -\frac{\partial p}{\partial x_i} + \frac{\partial \tau}{\partial x_j} + S_M \tag{3}$$

where i and j are indices, x_i represents the coordinates axes ($i = 1$–3 for x, y, z directions, respectively), ρ the density, t the time, U the velocity vector, p the pressure, τ the stress tensor, and S_M the momentum source.

ANSYS CFX uses an element-based finite volume method. The equations are discretized and solved iteratively for each control volume. Solution variables and fluid properties are stored at the nodes (mesh vertices), while control volumes are constructed around the mesh nodes.

For the advection and the transient schemes, the high-resolution option and the second order backward Euler scheme were selected, respectively. Further details may be obtained in the ANSYS CFX Manual [2].

The convergence of the solution was checked by monitoring the residuals for each equation at the end of each time step. Residuals are a measure of the local imbalance of each conservative control volume equation. The root mean square residual values were set to 10^{-4} for the mass and momentum variables.

Transient simulations were considered with a fix time step of 0.10 s. Around 7–8 iterations were required to reach the convergence criteria in each time step. The transient statistics were obtained once the steady state was reached.

Multiphase simulations were performed considering two different continuous fluids (air and water). Those phases are solved in the entire fluid domain. To solve the interaction of both fluids, the Eulerian–Eulerian multiphase flow homogeneous model was selected. With this model, a common flow field is shared by the air–water flow, as well as other relevant fields such as turbulence [2].

To track the interphase, the free surface model was selected. This model uses a compressive discretization scheme in the volume fraction advection scheme to keep the interface sharp. This control reduces the smearing at the free surface [2]. It was assumed that the free surface was located on the 0.5 air volume fraction. A surface tension model was considered with a surface tension coefficient of 0.072 N/m.

As symmetry in the transverse direction about the two cycles was observed in the experimental tests, only one of the two cycles was considered in the fluid domain. The inlet and outlet boundary conditions were located at 1.00 m (4.0P) upstream of the labyrinth weir and at 2.425 m (9.7P) downstream of the weir, respectively. The modeling boundary conditions were set as: hydrostatic pressures considering the water levels measured experimentally for each test at the inlet and outlet conditions; symmetry condition in the transverse direction; acrylic surface roughness in all the walls; atmosphere condition as an opening condition with a relative pressure of 0 Pa, water volume fraction of 0 and air volume fraction of 1. These boundary conditions were similar to those used by Savage et al. [29] to solve labyrinth weir flow with the CFD code FLOW-3D.

The Grid Convergence Index (GCI) [27] is not a direct measurement of the mesh accuracy; however, it does ensure with a level of confidence that the solution is approaching the mesh convergence solution, in the asymptotic range. With three mesh sizes, ASCE [3] recommends a factor of safety, $F_s = 1.25$. For testing the mesh convergence, the GCI values were computed using the mesh sizes shown in Table 1. Similarly to Savage et al. [29], the analysis was based on the discharge coefficient C_L, with GCI values lower than 1.0%.

Considering the obtained results, a mesh based on 0.015 m hexahedral elements was considered sufficiently insensitive to be used in this study. Special refinement near the wall (mesh size = 0.002 m) was considered in the weir crest to capture the overflow of the weir. With this mesh size, each simulation required around 18 h using an 8-core Intel(R) Xeon(R) CPU at 2.40 GHz. Figure 4 shows the free surface obtained by the code in free-flow condition, for $\alpha = 30°$ and $H_t/P = 0.86$.

Table 1 Mesh convergence for a discharge of 0.263 m³/s

Mesh size (m)	Discharge coefficient C_L (–)	Relative error (%)	Experimental result C_L (–)	Relative error against experimental data (%)	GCI (%)
0.025	0.504	–	0.495	1.78	–
0.020	0.498	1.14	0.495	0.62	2.53
0.015	0.498	0.06	0.495	0.56	0.48

Fig. 4 Simulation of free surface flow for sidewall angle $\alpha = 30°$ and $H_l/P = 0.86$
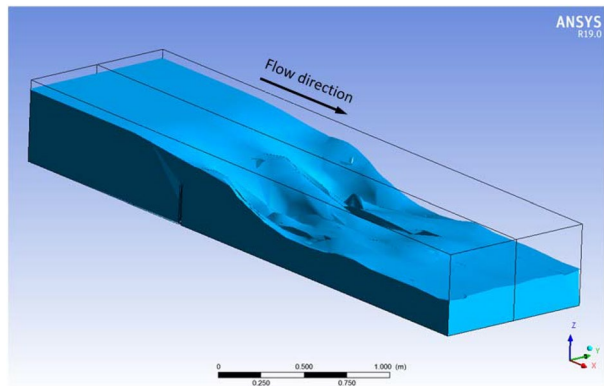
To predict the effect of turbulence without using a prohibitively fine mesh, Reynolds averaged Navier–Stokes (RANS) equations were used. The Eddy-viscosity turbulence models consider that such turbulence consists of small eddies which are continuously forming and dissipating, and in which the Reynolds stresses are assumed to be proportional to mean velocity gradients.

The Reynolds stresses obtained in the closure problem may be related to the mean velocity gradients and eddy dynamic viscosity by the gradient diffusion hypothesis:

$$-\rho \overline{u_i' u_j'} = \mu_t \left(\frac{\partial U_i}{\partial x_j} + \frac{\partial U_j}{\partial x_i} \right) - \frac{2}{3} \delta_{ij} \left(\rho k + \mu_t \frac{\partial U_k}{\partial x_k} \right) \tag{4}$$

with μ_t being the eddy dynamic viscosity or turbulent viscosity, $k = (1/2)\overline{u_i' u_i'}$ the turbulent kinetic energy and δ the Kronecker delta function.

The flow over the weir is expected to be dominated by gravity rather than by turbulence. However, nappe interference and instability was observed in free-flow labyrinth weirs (e.g., [8, 10]). Herein, three of the most usual two-equation RANS turbulence models were tested: the standard $k-\varepsilon$ model [19]; the Re-Normalisation Group (RNG) $k-\varepsilon$ model [41]; and the $k-\omega$ based Shear–Stress Transport (SST) model [26].

5 Results and discussion

5.1 Free-flow discharge coefficient

A total of 21 simulations were performed in free-discharge flow. Figure 5 shows a comparison of the numerical results obtained with three different turbulence models and the experimental data. The random error of the discharge coefficient was estimated from the formula of propagation of error, taking into account the experimental random errors in discharge, length of the weir and head, as per Falvey [13] and Lopes [20]. Therein, Eq. (1) was used to obtain the labyrinth discharge relationship.

In general, no remarkable differences were observed between the three turbulence models. This may indicate that the discharge is dominated by gravitational effects rather than by turbulence, for such geometric and hydraulic conditions. In general, the numerical results were found to fall within the random error interval. The standard deviation σ of the relative error of C_L was smaller than 0.011 for $H_t/P \geq 0.30$. The SST turbulence model yielded results slightly more accurate than the other turbulence models ($\sigma_{\kappa-\varepsilon} = 0.011$; $\sigma_{RNG\,\kappa-\varepsilon} = 0.008$; $\sigma_{SST} = 0.006$).

In Fig. 6, the experimental data by Lopes [20] and numerical results are compared with data available in the literature. For $H_t/P \geq 0.30$, maximum relative differences with experimental data were smaller than 2.4% for the $\kappa-\varepsilon$ turbulence model, and smaller than 1.0% for the SST and the RNG $\kappa-\varepsilon$ turbulence models.

Formulae obtained by several authors were also plotted in Fig. 6. The numerical results are close to those obtained by interpolating the 20° and 35° curves proposed by Crookston and Tullis [9]. The formulae proposed by Vatankhah [37] also fits well to the data by Lopes [20] for $H_t/P > 0.40$, albeit giving slightly larger values of C_L for $0.20 < H_t/P < 0.40$. In turn, once readjusted to consider the total centerline crest length, the experimental values obtained by Khode et al. [18], and the curves developed based on such data [18, 38], are relatively smaller than the values obtained by Lopes [20]. Based on Falvey [13], such an order of magnitude of the relative differences would be expected, considering that the Khode et al. [18] data was obtained for a weir height lower than or equal to 0.10 m. For larger values of H_t/P, all the methods tend to similar results.

Fig. 5 Comparison of experimental and numerical free-flow discharge coefficient C_L for sidewall angle $\alpha = 30°$
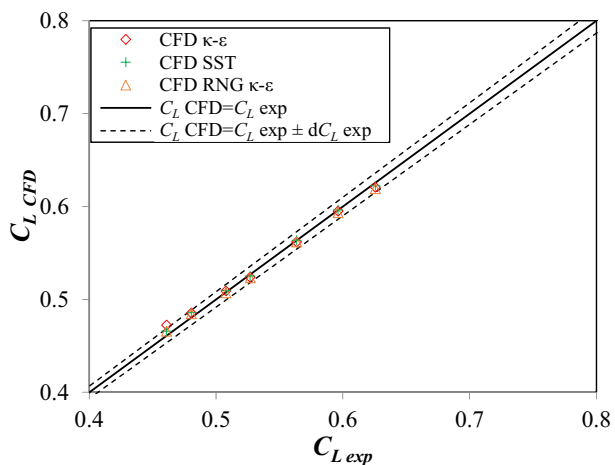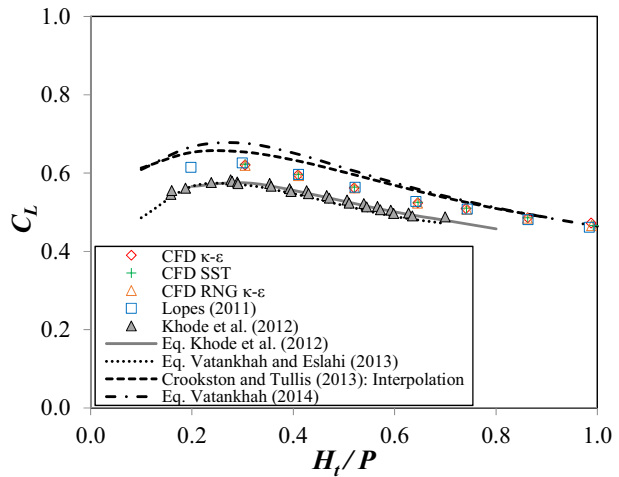
Fig. 6 Comparison of experimental and numerical free-flow discharge coefficient C_L versus H_t/P for sidewall angle $\alpha = 30°$ (Data of Khode et al. [18] obtained through digitalization)


5.2 Free surface profile upstream of the weir

Figure 7 shows the approaching free surface profiles obtained in the middle of one cycle and in the center of the flume (i.e., in the middle of two cycles). For each test, free surface elevations over the weir crest were normalized with the depth of flow over the weir crest (h/h_0). The horizontal distance was normalized considering the labyrinth weir height (x/P). The results suggest that the approaching free surface profile upstream of the labyrinth weir may be considered independent of the normalized head (H_t/P). On the other hand, the influence of the normalized head on the dimensionless free surface profile is noticeable downstream of the labyrinth weir.

5.3 Flow depth downstream of the weir

Flow depths downstream of the labyrinth weir were analyzed for $H_t/P = 0.86$, corresponding to a subcritical flow regime. Using a conductivity probe, Lopes [20] obtained characteristic depths y_{90} in the center of the flume (between two cycles) and in the center of one cycle. For this study, the characteristic depth y_{10} was also calculated, as an indicative value of the minimum unsteady flow depth at a given location, in the absence of air entrainment. In addition, maximum and minimum flow depths near the flume wall, obtained by visual observation, were collected. Figure 8 shows a comparison of the three turbulence models and the laboratory measurements. Transient statistics were obtained once the numerical model reached steady state conditions. Due to the relatively large mesh size used to solve the entire domain (0.015 m mesh size), considerable differences were found in the vicinity of the weir. This suggests that the free falling and impact jet regions would require a finer mesh size to provide better accuracy. However, the general behavior of the flow downstream of the jet impact region, where 3D effects become less marked (i.e., for distances to its downstream face > 0.6–0.8 m), was reasonably well captured by the numerical model. Shortly downstream of the labyrinth weir, the $\kappa - \varepsilon$ turbulence model gave better results in the center of the flume, while the RNG $\kappa - \varepsilon$ turbulence model was more accurate in the center of the cycle. Downstream of the

Fig. 7 Normalized free surface elevation over the weir crest for free-flow conditions: **a** center of the flume; **b** Center of the cycle
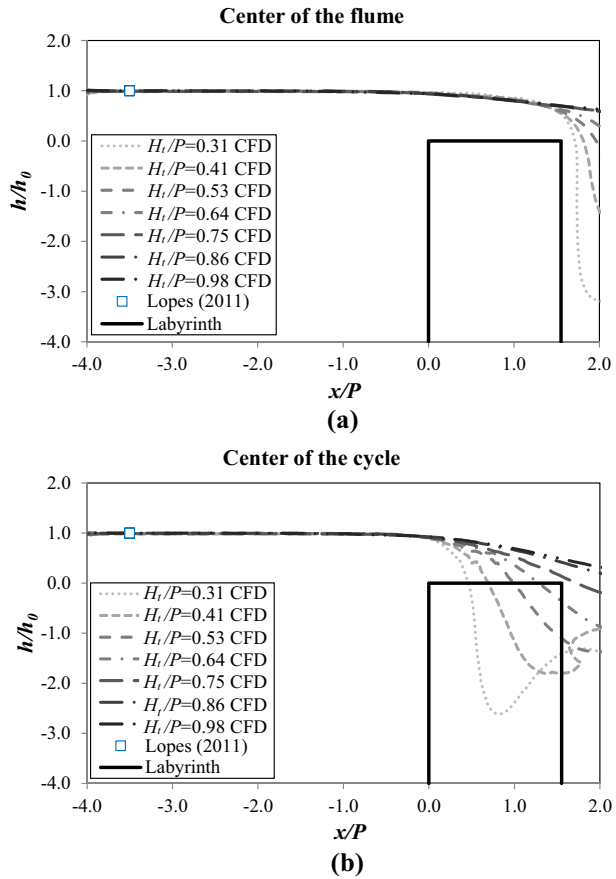
near-weir region, the flow depths predicted by the three turbulence models were generally close to their experimental counterparts.
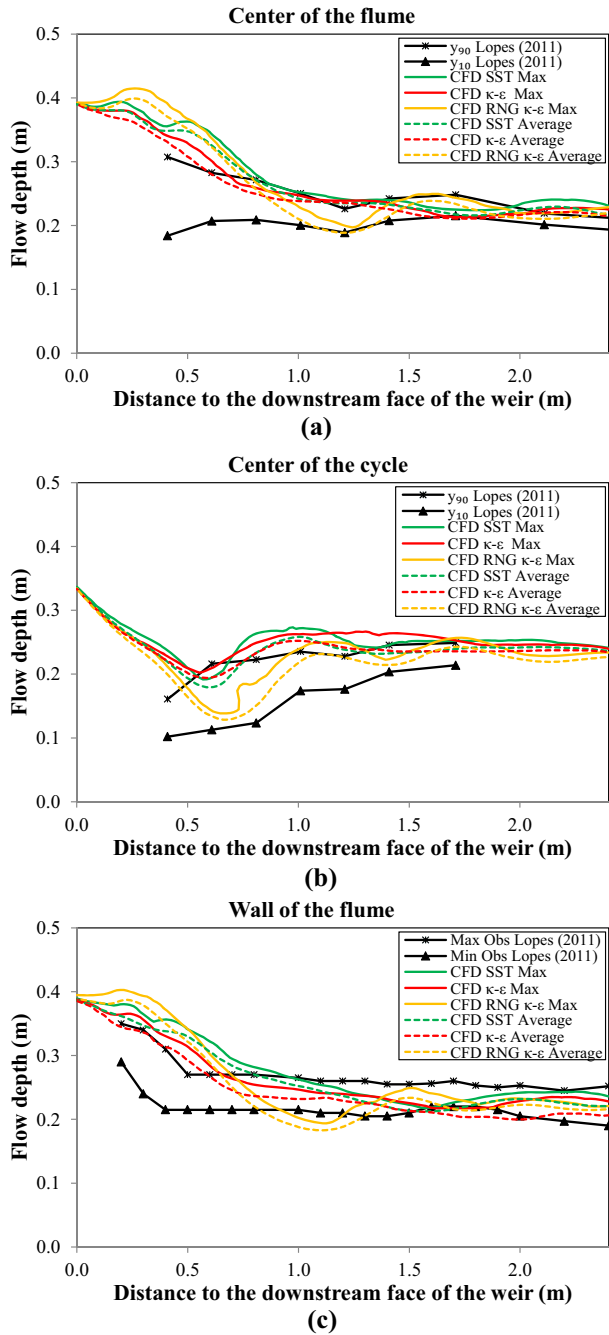
5.4 Submerged-flow discharge coefficient

Following Tullis et al. [36], the effect of submergence on the discharge relationship of labyrinth weirs may be analyzed considering the submerged upstream total head normalized by H_t (H^*/H_t) as a function of the downstream submergence total head normalized by H_t (H_d/H_t), as shown in Fig. 1. In total, 80 simulations were analyzed in submerged discharge conditions.

Considering Eq. (1) and replacing H_t with H^*, the experimental and numerical discharge coefficients were compared for the same level of submergence. Figure 9 shows the comparison of C_L obtained with three different turbulence models, for three H_t/P values and various submergence levels. The random error of the discharge coefficient was also computed.

Overall, very good agreement was obtained with the three turbulence models for different submergence levels, also suggesting that the submerged discharge is mainly dominated by gravitational effects. The order of magnitude of the relative differences between the numerical results and experimental data was similar to that given by

Fig. 8 Flow depth downstream of the weir crest for free-flow conditions, for $H_t/P = 0.86$: **a** center of the flume; **b** Center of the cycle; **c** Wall of the flume
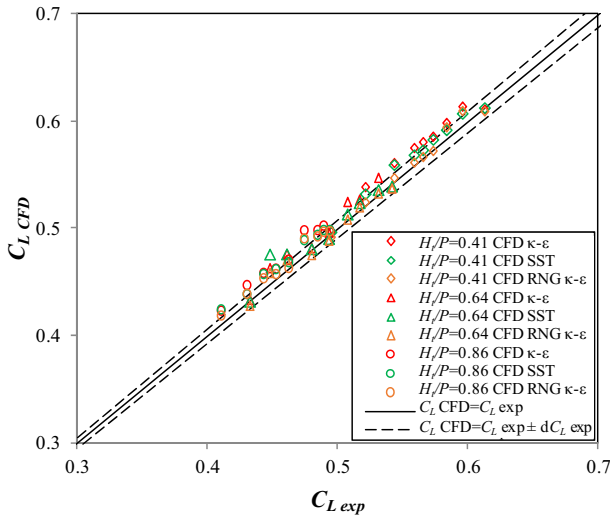
Fig. 9 Comparison of experimental and numerical submerged-flow discharge coefficient C_L for a sidewall angle $\alpha = 30°$

random errors. The RNG κ-ε turbulence model gave slightly more accurate results than the other models, giving maximum relative differences with experimental data of less than 3.6% ($\sigma_{RNG\ \kappa-\varepsilon} = 0.013$). Maximum relative differences for the $\kappa - \varepsilon$ and SST turbulence models were less than 5.2% and 6.2%, respectively ($\sigma_{\kappa-\varepsilon} = 0.014$; $\sigma_{SST} = 0.015$).

Figure 10 shows the experimental and numerical dimensionless head results obtained in submergence conditions. Very good agreement was found with the experimental data
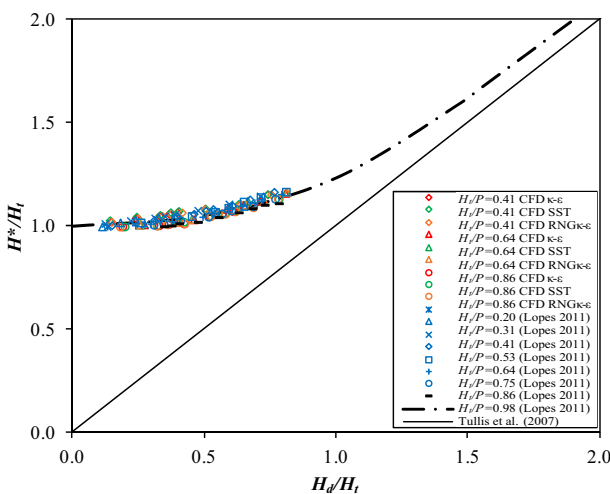

Fig. 10 Comparison of experimental and numerical dimensionless submerged hydraulic head relationship, H^*/H_t versus H_d/H_t, for submerged labyrinth weirs with a sidewall angle $\alpha = 30°$

presented in Lopes et al. [21] and the piecewise function proposed by Tullis et al. [36], regardless of the submergence level.

6 Conclusions

In this study, results of the discharge coefficient on free and submerged flows over labyrinth weirs for a large sidewall angle were analyzed from experimental studies and numerical simulations using a commercially available computational fluid dynamics (CFD) software, for three different turbulence models. The free surface flow profile was also analyzed in the upstream and downstream reaches of the labyrinth weir.

Specific results of this study include the following:

- Several formulae have been proposed to date to estimate the discharge coefficient of labyrinth weirs, namely for free-flow conditions. In general, the experimental data and related regression curves, for an identical sidewall angle, provide similar values of C_L for moderate to large H_t/P ratios.
- Very good agreement was found between the experimental data and numerical results of the discharge coefficient, with the maximum relative differences being lower than 1% for free-flows and 3.6% for submerged flow conditions, when the RNG κ-ε turbulence model is considered.
- In free-flow conditions, the normalized free surface profile upstream of the labyrinth weir was virtually independent of the total head to weir height ratio.
- The flow depth downstream of the labyrinth weir was simulated with reasonably good agreement in free, subcritical flow conditions. However, a finer mesh resolution should be adopted to improve its accuracy near the overflow structure, where differences among the turbulence models were also considerable.
- In submerged-flow conditions, the CFD results of the dimensionless submerged head, for various turbulence models, closely followed the experimental data by Lopes [20], as well as the regression curve proposed by Tullis et al. [36]. The results suggest that the discharge coefficient in free-flow and submerged conditions is dominated by gravitational forces for 30° labyrinth weirs, under such flow conditions, while the choice of the turbulence model has a limited effect on the discharge coefficient, similarly to the findings of Savage et al. [29], for the computed discharge in free-flow over a 15° labyrinth spillway.

In conclusion, CFD models may provide very good predictions of the discharge on free and submerged labyrinth weirs for a large sidewall angle. The flow depths downstream of the weir can also, numerically, be captured well. However, the accurate modeling of the complex air–water flow downstream of the weir, in particular in its vicinity, remains a challenge for further research.

References

1. Azimi AH (2013) Discussion of 'Experimental studies on flow over labyrinth weir' by B. V. Khode, A. R. Tembhurkar, P. D. Porey, and R. N. Ingle. J Irrig Drain Eng 139(12):1051–1053
2. ANSYS Inc. (2016) ANSYS CFX. Solver Theory Guide. Release 18.0
3. ASCE Task committee on 3D free-surface flow model verification and validation (2009) Verification and validation of 3D free-surface flow models. Environmental and Water Resources Institute (EWRI), Reston, VA
4. Bilhan O, Cihan Aydin M, Emin Emiroglu M, Miller CJ (2018) Experimental and CFD analysis of circular labyrinth weirs. J Irrig Drain Eng 144(6):04018007
5. Boileau P (1854) Traité de la mesure des eaux courantes, ou, Expériences, observations et méthodes concernant les lois des vitesses, le jaugeage et l'évaluation de la force mécanique des cours d'eau de toute grandeur, le débit des pertuis usines, des fortifications et des canaux d'irrigation, et l'action dynamique des courants sur les corps en repos. Mallet-Bachelier, Gendre et Successeur de Bachelier, Paris, France
6. Crookston BM (2010) Labyrinth weirs. Ph.D. Thesis, Utah State University, Logan, UT, USA
7. Crookston BM, Anderson RM, Tullis BP (2018) Free-flow discharge estimation method for Piano Key weir geometries. J Hydro-environ Res 19:160–167
8. Crookston BM, Tullis BP (2012) Labyrinth weirs: nappe interference and local submergence. J Irrig Drain Eng 138(8):757–765
9. Crookston BM, Tullis BP (2013) Hydraulic design and analysis of labyrinth weirs I: discharge Relationships. J Irrig Drain Eng 139(5):363–370
10. Crookston BM, Tullis BP (2013) Hydraulic design and analysis of labyrinth weirs II: nappe aeration, instability, and vibration. J Irrig Drain Eng 139(5):371–377
11. Darvas LA (1971) Discussion of 'Performance and design of labyrinth weirs', by Hay and Taylor. J Hydraul Eng 97(80):1246–1251
12. Denys F, Basson G (2018) Transient hydrodynamics of Piano Key weirs. In: 7th IAHR international symposium on hydraulic structures, Aachen, Germany
13. Falvey HT (2003) Hydraulic design of Labyrinth Weirs. ASCE Press, Reston
14. Gupta SK, Singh VP (2013) Discussion of 'Experimental studies on flow over labyrinth weir' by B. V. Khode, A. R. Tembhurkar, P. D. Porey, and R. N. Ingle. J Irrig Drain Eng 139(12):1051–1053
15. Hager WH, Pfister M, Tullis BP (2015) Labyrinth weirs: developments until 1985. In: Proceedings of 36th IAHR World Congress, The Hague, The Netherlands
16. Hay N, Taylor G (1970) Performance and design of labyrinth weirs. J Hydraul Eng 96(11):2337–2357
17. Houston KL (1983) Hydraulic model study of Hyrum Dam auxiliary labyrinth spillway. Report No. GR 82-13, U.S. Bureau of Reclamations, Denver, Colorado
18. Khode BV, Tembhurkar AR, Porey PD, Ingle RN (2012) Experimental studies on flow over Labyrinth Weir. J Irrig Drain Eng 138(6):548–552
19. Launder BE, Sharma BI (1972) Application of the energy dissipation model of turbulence to the calculation of flow near a spinning disc. Lett Heat Mass Transf 1(2):131–138
20. Lopes R (2011) Capacidade de vazão, energia específica residual e caracterização do escoamento de emulsão ar-água em soleiras descarregadoras em labirinto. Ph.D. thesis, Instituto Superior Técnico, Universidade Técnica de Lisboa, Lisbon, Portugal **(in Portuguese)**
21. Lopes R, Matos J, Melo JF (2009) Discharge capacity for free-flow and submerged labyrinth weirs. In: Proceeding 33rd IAHR congress: water engineering for a sustainable environment, Vancouver, Canada
22. Lopes R, Matos J, Melo JF (2011) Flow properties and residual energy downstream of labyrinth weirs. In: Erpicum S, Laugier F, Boillat J-L, Pirotton M, Reverchon B, Schleiss A (eds) Labyrinth and piano key weirs—PKW 2011. CRC Press, Leiden, pp 97–104
23. Lux F, Hinchliff DL (1985) Design and construction of labyrinth spillways. In: Proceedings of the 15th congress ICOLD, vol 4, Q59-R15, Lausanne, Switzerland, pp 249–274
24. Magalhães AP, Lorena M (1989) Hydraulic design of labyrinth weirs. Rep. No. 736, National Laboratory of Civil Engineering, Lisbon, Portugal
25. Matos J, Frizell, KH (1997) Air concentration measurements in highly turbulent aerated flow. In: Wang SSY, Carstens T (eds) Proceedings of the 27th IAHR congress, San Francisco, USA, vol 1, pp 149–154
26. Menter FR (1994) Two-equation eddy-viscosity turbulence models for engineering applications. AIAA J 32(8):1598–1605
27. Roache PJ (1997) Quantification of uncertainty in computational fluid dynamics. Annu Rev Fluid Mech 29:123–159

28. Salazar F, Mauro JS, Oñate E, Toledo M (2015) CFD analysis of flow pattern in labyrinth weirs. In: Dam Protections against Overtopping and Accidental Leakage—proceedings of the 1st international seminar on dam protections against overtopping and accidental leakage, Madrid, Spain
29. Savage BM, Crookston BM, Paxson GS (2016) Physical and numerical modeling of large headwater ratios for a 15° labyrinth spillway. J Hydraul Eng 142(11):04016046
30. Schleiss AJ (2011) From Labyrinth to Piano Key weirs—a historical review. In: Proceedings of the international conference on Labyrinth and Piano Key Weirs, Liege, Belgium
31. Taylor G (1968) The performance of labyrinth weirs. Ph.D. thesis, University of Nottingham, UK
32. Torres C, Borman D, Sleigh A, Neeve D (2017) Three dimensional numerical modelling of full-scale hydraulic structures. In: Proceedings of the 37th IAHR world congress, Kuala Lumpur, Malaysia, pp 1335–1343
33. Torres C, Borman D, Sleigh A, Neeve D (2018) Determination of scale effects for a scaled physical model of a Labyrinth weir using CFD. In: 7th IAHR international symposium on hydraulic structures, Aachen, Germany
34. Tullis BP (2018) Size-scale effects of labyrinth weir hydraulics. In: 7th IAHR international symposium on hydraulic structures, Aachen, Germany
35. Tullis JP, Nosratollah A, Waldron D (1995) Design of labyrinth spillways. J Hydraul Eng 121(3):247–255
36. Tullis B, Young J, Chandler M (2007) Head-discharge relationships for submerged labyrinth weirs. J Hydraul Eng 133(3):248–254
37. Vatankhah AR (2014) Discussion of 'Hydraulic design and analysis of labyrinth weirs. I: discharge relationships' by B. M. Crookston and B. P. Tullis. J Irrig Drain Eng. https://doi.org/10.1061/(asce)ir.1943-4774.0000751
38. Vatankhah AR, Eslahi N (2013) Discussion of 'Experimental studies on flow over labyrinth weir' by B. V. Khode, A. R. Tembhurkar, P. D. Porey, and R. N. Ingle. J Irrig Drain Eng 139(12):1051–1053
39. Villemonte JR (1947) Submerged-weir discharge studies. Eng News Rec 866:54–57
40. Willmore CM (2004) Hydraulic characteristics of labyrinth weirs. M.S. Report, Utah State University, Logan, UT, US
41. Yakhot V, Smith LM (1992) The renormalization group, the ε-expansion and derivation of turbulence models. J Sci Comput 7(1):35–61